

# Periosteum-Mimetic Structures Made from Freestanding Microgrooved Nanosheets

Xuetao Shi, Toshinori Fujie, Akihiro Saito, Shinji Takeoka, Ying Hou, Yiwei Shu, Mingwei Chen, Hongkai Wu,\* and Ali Khademhosseini\*

Bone remodeling is a complex and well-orchestrated process that requires the cooperation of various types of cells (e.g., osteoblasts, endothelial cells, and stem cells) from the bone marrow, bone matrix, and periosteum.<sup>[1]</sup> However, most tissue engineering platforms for bone repair and regeneration neglect the importance of the periosteum, which is a thin membrane that encases the surfaces of most bones.<sup>[2]</sup> In adults, the periosteum is in a quiescent state and only provides mechanical support to tendons; however, the stem cells residing on the periosteum are activated to form the osteoblasts necessary for reconstructing injured bones.<sup>[2]</sup> The inner cellular layer of the periosteum plays a key role in bone regeneration.<sup>[3]</sup> It possesses an exquisite topographic surface that consists of longitudinally oriented cells and collagen fibers.<sup>[3]</sup> These unique characteristics of the periosteum harness and regulate cell arrangement, collagen fiber alignment,

and the direction of bone development. The potential of the periosteum regarding the growth modulation of bone has been verified *in vitro* and *in vivo*. The failure of the periosteum in patients who suffer bone defects induced by tumor or trauma poses a considerable challenge.<sup>[4]</sup> Creating an artificial scaffold that presents the conditions and morphology necessary to simulate the native periosteum may be an ideal approach for these cases.

Due to the increasing awareness of the periosteum's importance, numerous recent studies have constructed tissue engineered periosteum using collagen and hydrogels.<sup>[5]</sup> However, most of these studies have neglected the hierarchical topographic surface of the periosteum, which is important for bone elongation. Importantly, such artificial periosteum films cannot effectively anchor to or integrate with bone scaffolds (e.g., autografts, allografts, and artificial porous scaffolds), which can lead to serious complications during clinical interventions. Inspired by the unique features of nanoscale materials, freestanding polymeric ultrathin film (referred as "nanosheet") may be a promising candidate for generating artificial periosteum. Nanosheets are typically tens of nanometers in thickness and several centimeters in surface area. Due to their ultrathin structure, they have a number of desirable properties, such as noncovalent adhesiveness, facile transferability, selective molecular permeability, and excellent transparency.<sup>[6]</sup> These properties allow the nanosheets to be used in many applications, such as nanosensors, wound dressings, and filtration membranes.<sup>[7]</sup> A nanosheet produced by a biodegradable polymer has also attracted considerable interest in surgical applications. Poly(lactic acid) nanosheets have been successfully developed and clinically used in the treatment of burn wounds.<sup>[8]</sup> Compared with poly(lactic acid), poly(lactic-co-glycolic acid) (PLGA) has improved biodegradability, which may facilitate the generation of material-free cell sheets.<sup>[9]</sup>

The cells and extracellular matrix (ECM) in human tissues and organs are organized in an exquisite and hierarchical manner.<sup>[10]</sup> Micropatterning is a powerful technique to create various motifs on flat and curved substrates.<sup>[11]</sup> In addition to its use in electronics, micropatterning has become an effective approach to create miniaturized structures for constructing functional tissue and fundamental research in cell biology.<sup>[12]</sup> By using micropatterning, different motifs have been generated on substrates, such as glass and poly(dimethylsiloxane) (PDMS), and biopolymers, such as PLGA, to build two-dimensional tissues (e.g., skin) and three-dimensional tissues (e.g., blood vessels and cardiac tissue).<sup>[13]</sup>

In this study, to recapitulate the organized microscale structure in periosteum, we used micropatterning to create topographic cues on the surface of PLGA nanosheets for regulating

Dr. X. T. Shi,<sup>[†]</sup> Dr. T. Fujie,<sup>[†]</sup> Dr. Y. Hou, Prof. M. W. Chen, Prof. H. K. Wu, Prof. A. Khademhosseini  
WPI-Advanced Institute for Materials Research  
Tohoku University  
Sendai 980-8578, Japan  
E-mail: chhkwwu@ust.hk; alik@rics.bwh.harvard.edu



Dr. T. Fujie, Dr. A. Saito, Prof. S. Takeoka  
Department of Life Science and Medical Bioscience  
Graduate School of Advanced Science and Engineering  
Waseda University  
Tokyo, Japan

Y. Shu, Prof. H. K. Wu  
Department of Chemistry & Division of Biomedical Engineering  
Hong Kong University of Science & Technology  
Hong Kong, China

Prof. A. Khademhosseini  
Center for Biomedical Engineering  
Department of Medicine, Brigham and Women's Hospital  
Harvard Medical School; Harvard-MIT Division of Health Sciences  
and Technology  
Massachusetts Institute of Technology  
Wyss Institute for Biologically Inspired Engineering  
at Harvard University  
Boston, MA 02115, USA

Prof. A. Khademhosseini  
Department of Maxillofacial Biomedical Engineering  
and Institute of Oral Biology  
School of Dentistry  
Kyung Hee University  
Seoul 130-701, Republic of Korea

Prof. A. Khademhosseini  
Department of Physics  
King Abdulaziz University  
Jeddah 21569, Saudi Arabia

<sup>[†]</sup>These authors contributed equally to this work.

DOI: 10.1002/adma.201305804

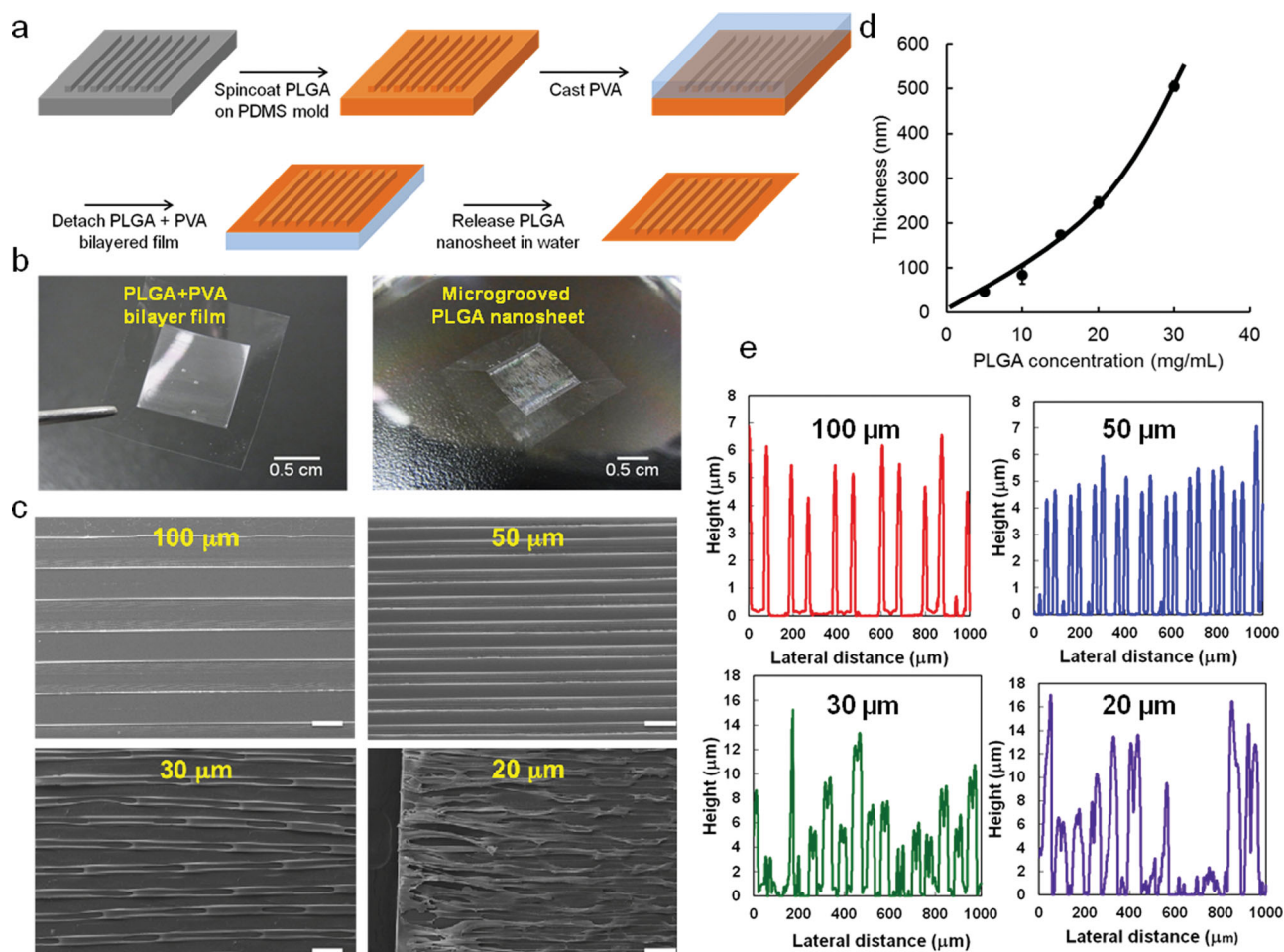


**Figure 1.** Generation of microgrooved PLGA nanosheets. a) A schematic for the fabrication of microgrooved PLGA nanosheets. b) Images of the PLGA and PVA bilayer film and the microgrooved PLGA nanosheet. c) SEM images of PLGA nanosheets with different groove spacings (scale bars: 100  $\mu\text{m}$ ). d) Thickness of flat part of PLGA nanosheets fabricated with different PLGA concentrations. e) The height of the microgrooved PLGA nanosheets with different groove widths using a 10 mg/mL PLGA solution; and the groove spacing is 100 (in red color), 50 (in blue color), 30 (in green color), and 20 (in purple color)  $\mu\text{m}$ .

cell and ECM arrangement in a manner similar to natural periosteum. We propose that this freestanding nanosheet can be stably anchored onto various tissue engineering scaffolds for bone repair for the maintenance of topographical surface morphologies. The development of periosteum biomimics for tissue engineering applications may provide an innovative strategy for bone regenerative therapies.

Freestanding PLGA nanosheets with microgrooved patterns were fabricated using a facile procedure (Figure 1a). Initially, PLGA nanosheets were prepared by spin coating 10 mg/mL PLGA-dichloromethane solution on a PDMS negative replica with microgrooved motifs. Then, a poly(vinyl alcohol) (PVA) supporting layer was cast onto the PLGA nanosheet. The microgrooved PLGA nanosheets supporting the PVA layer were removed from the PDMS mold by tweezers and were then placed into a PBS solution to dissolve the PVA layer (Figure 1b). Finally, the freestanding PLGA nanosheets were transferred to the surfaces of the proposed scaffolds.

PLGA nanosheets with microgrooved and pillar motifs on their surfaces were successfully fabricated using the

forementioned method. The morphologies of the nanosheets were imaged using a scanning electron microscope (SEM). As shown in Figure 1c, the microscale structure inherited from the PDMS replicate was printed onto the PLGA nanosheets with well-resolved groove spacings of 30, 50 and 100  $\mu\text{m}$ . However, the PLGA nanosheet with a groove spacing of 20  $\mu\text{m}$  was not successfully produced. The microgroove spacing may have been too small for this size, allowing increased fusion of the neighboring grooves when the PDMS mold was peeled from the surface of the nanosheet. Although the technique used in this work is not suitable to fabricate nanosheets with small groove spacings (less than 30  $\mu\text{m}$ ); a micropattern with a groove spacing of 50  $\mu\text{m}$  is enough for harnessing cell alignment. In addition, we measured the height of the flat parts of the nanosheets (Figure 1d). The height of the flat part of the nanosheets using a 10 mg/mL PLGA solution is 84 nm. When we increased the PLGA concentration, the height of the nanosheets significantly increased. In contrast to the traditional groove-and-ridge motifs, the ridge area of the achieved microgrooved PLGA nanosheets also exhibited a smaller groove-and-ridge

morphology (Figure 1e & Figure S1). For the PLGA nanosheets with a groove spacing of 30  $\mu\text{m}$ , the ridge heights varied significantly due to sunken regions on some of the ridges. This morphology can be observed in the SEM images. For the PLGA nanosheets with groove spacings of 50 and 100  $\mu\text{m}$ , the profiles of the heights in the micropatterns exhibited two narrow peaks instead of one flat peak, as in the PDMS replica. We postulate that the middle of the ridge area sank and that the left and right walls of the ridge were maintained. This phenomenon may be due to the evaporation of dichloromethane and the residual PLGA maintaining its groove-and-ridge morphology. Therefore, the inside of the ridge area appears hollow, and the ridge areas of the nanosheets with larger groove spacings sank more easily as a result. This was verified by the SEM image of the nanosheet with pillars. As shown in Figure S2, the pillars on the PLGA nanosheet were hollow. This unique grooved-and-ridge morphology facilitates cell residence. The cells can not only be seeded onto the groove area but also propagate along the sunken ridge area (Figure S3). However, the cells preferred to reside in the groove area for the typical grooved-and-ridge morphology.

An interesting aspect of nanosheet is its noncovalent adhesiveness onto different substrates. Flat nanosheets have previously been demonstrated to adhere to the surface of substrates, such as Petri dishes and skin.<sup>[14,6a]</sup> Their noncovalent adhesiveness is exhibited by decreasing film thickness less than 200 nm due to the increment of film flexibility.<sup>[7b]</sup> Therefore, such a

flexible nanosheet with physical adhesiveness can be patched for the surface modification like a “sticker”. We used bone to investigate the adhesiveness and stability of microgrooved PLGA nanosheets in pursuit of two main purposes. First, flat nanosheets have been verified to stick tightly to dry surfaces. For tissue engineering applications, this unique property should also work in a hydrous milieu (e.g., live bone). Second, although many artificial bone scaffolds have been developed, autograft bone is considered the golden standard and remains the safest and fastest clinical intervention for bone repair.<sup>[15]</sup> Therefore, investigating the interplay between pseudo-periosteum (microgrooved PLGA nanosheet) and bone is a worthwhile avenue of research. Herein, we covered a chicken humeral bone with a microgrooved PLGA nanosheet (Figure 2a and 2b). After 14 days of incubation in PBS solution, the microgrooved PLGA nanosheet remained tightly adhered to the bone surface without significant deformation, which is beneficial in regulating cell propagation and cell arrangement on the nanosheet (Figure 2c). The periosteum tightly covers the surface of bone.<sup>[2]</sup> The results verified that the developed nanosheet can simulate this property. In addition to simulating pristine periosteum, the noncovalent adhesion between the nanosheets and their substrates could facilitate applications in the clinic because the orthopedist would know that the thin nanosheets can withstand implants that are used for bone repair, such as autografts or scaffolds. By using microscratching test,<sup>[7b]</sup> we also investigated the physical adhesiveness of nanosheets of different PLGA

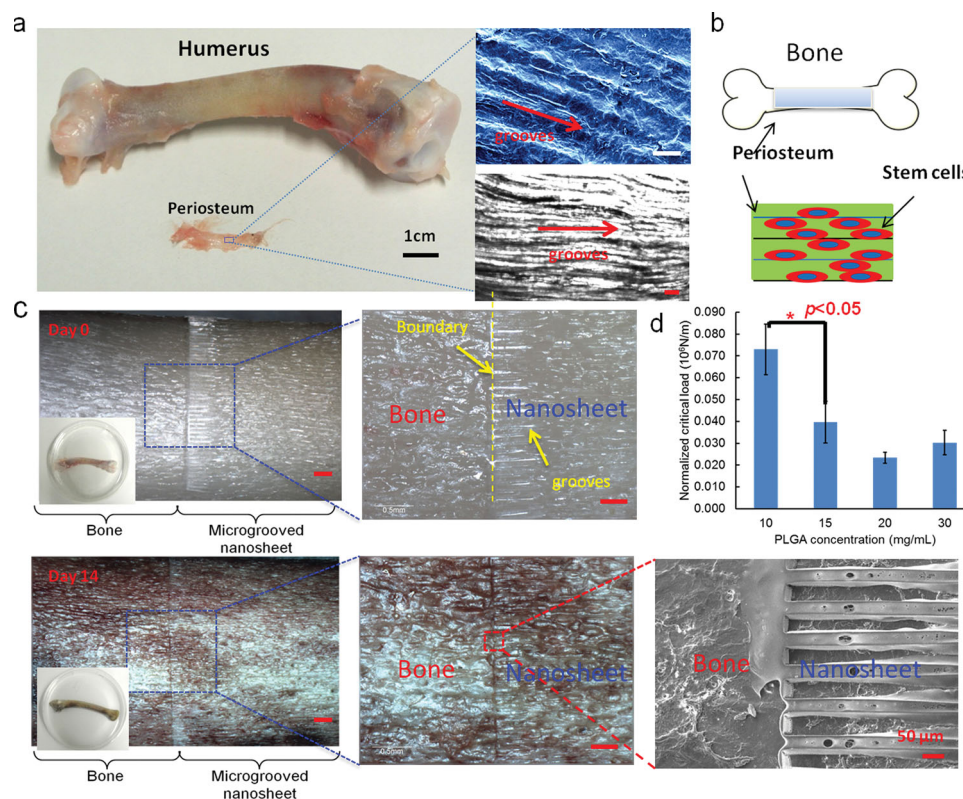


**Figure 2.** Physical adhesiveness of periosteum-like microgrooved PLGA nanosheets on bone. a) SEM and optical images of periosteum derived from the humerus of chicken (scale bars: 100  $\mu\text{m}$ ). b) A schematic of the morphology of periosteum and cell arrangement on periosteum. c) Images of microgrooved PLGA nanosheets adhered on the surfaces of bones before and after incubation in PBS solution for 14 days (scale bars: 500  $\mu\text{m}$ ). d) The physical adhesiveness of PLGA nanosheets fabricated from different PLGA concentrations.

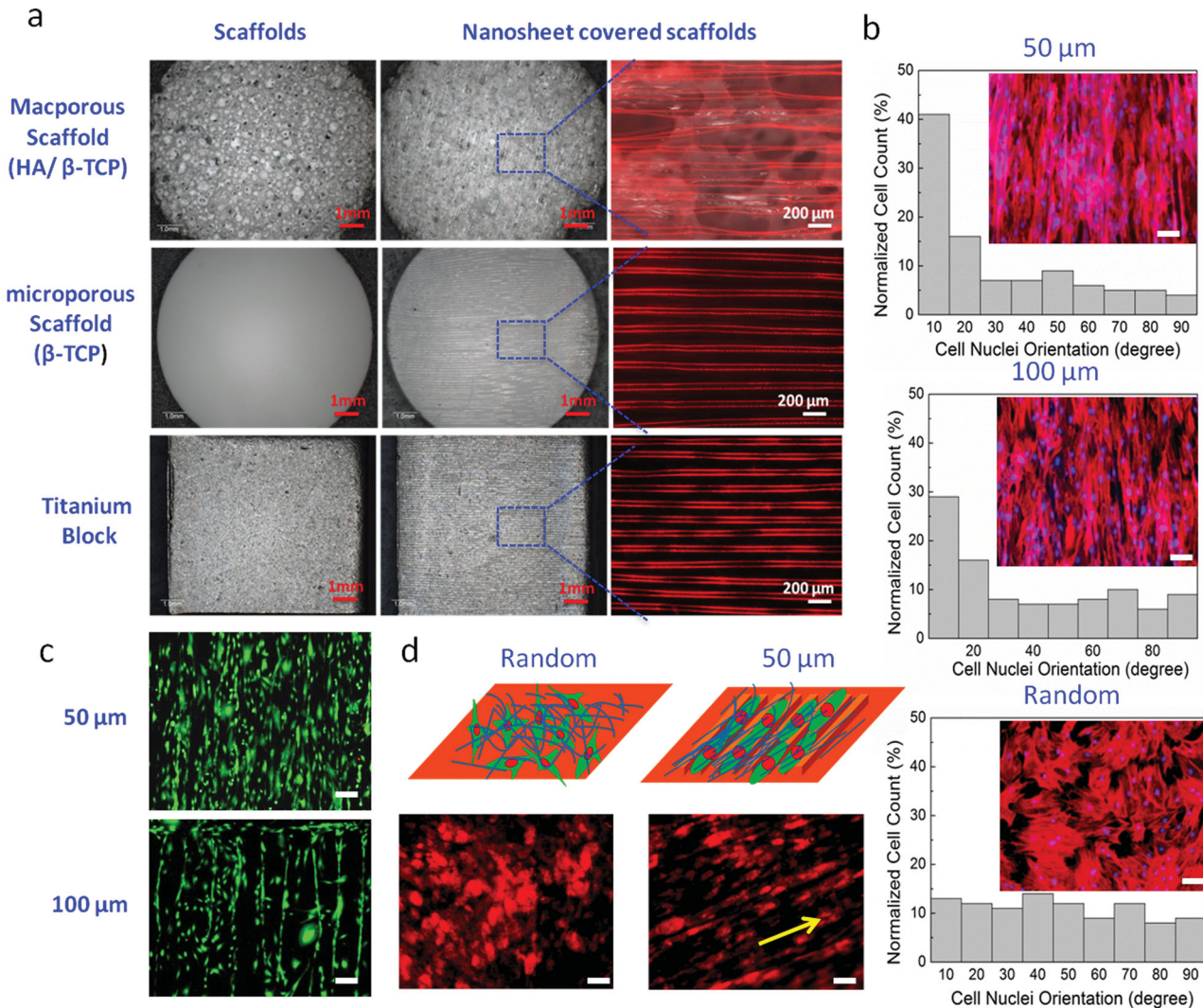


**Figure 3.** Microgrooved PLGA nanosheets adhered to various tissue engineering scaffolds. a) Images of microgrooved PLGA nanosheet-covering scaffolds (red fluorescent displays rhodamine-labelled PLGA nanosheets). b) The cell alignments on PLGA nanosheets with different groove widths and flat PLGA nanosheets (Random) after 3 days of culture (scale bars: 100 μm). c) Images of cells on PLGA nanosheets with different groove widths after 1 day of culture using LIVE/DEAD staining (scale bars: 100 μm). d) The alignment of type I collagen secreted by cells cultured on flat PLGA nanosheets (Random) and microgrooved PLGA nanosheets after 7 days of culture (the groove width is 50 μm; scale bars: 50 μm).

concentrations to SiO<sub>2</sub> substrates (Figures 2d and S4). The ability of nanosheets to resist scratch loads decreased with increasing PLGA concentration. The nanosheet obtained using a 10 mg/mL PLGA solution resisted significantly higher critical scratch load compared to the other groups, indicating the highest adhesiveness. When we decreased the PLGA concentration to 5 mg/mL, dispersed ribbons were generated inside the microgrooved nanosheet due to its extremely thin thickness in the grooved area. Therefore, we used the nanosheet fabricated by a 10 mg/mL PLGA solution for cell evaluation.

Next, microgrooved PLGA nanosheets were transferred onto common bone tissue engineering scaffolds and bone implants, including a macroporous hydroxyapatite/β-tricalciumphosphate (HA/β-TCP, the average pore size was 200–400 μm and the average porosity was 83%) scaffold, microporous β-TCP scaffold (pore size was less than 20 μm), and titanium block (Figures 3a

and S5). The microgrooved PLGA nanosheets firmly adhered to the surface of these scaffolds. Interestingly, similar to the nanosheet on bone, the nanosheets on these scaffolds were difficult to detach after they dried, even after being immersed in culture media. To observe the surface morphology of the nanosheet-covered scaffolds, we mixed rhodamine B with the PLGA solution during the fabrication of the nanosheets. The fluorescence images illustrate that the groove-and-ridge morphology was well maintained on the surfaces of the different scaffolds.

It has been long assumed that microgrooved patterns could harness the osteogenic differentiation of stem cells.<sup>[16]</sup> Many techniques have been developed to create a topographic surface on various materials. Microcontact printing techniques have been used to functionalize the surfaces of flat titanium and hydroxyapatite block with cell adhesive proteins and ECM.

Micropatterns and nanopatterns with grooved structures have been created by high-temperature casting and chemical etching.<sup>[17]</sup> However, the stability of the micropatterns and the complicated process limited their applications in bone repair. In addition, most of these methods could not create grooved surfaces on microporous scaffolds. Our results suggest that the nanosheets can overcome all of the aforementioned limitations and could thus be an excellent tool to create topographic motifs on various surfaces to control the behavior of cells.

We investigated the effect of PLGA nanosheets adhered to titanium blocks on cell morphology using human adipose-derived mesenchymal stem cells (ADMSCs). These cells were selected due to their rapid proliferation and because their harvesting requires minimally invasive techniques (Figures 3b–c, S6, and S7).<sup>[18]</sup> To promote cell attachment, we treated the surface with a 50  $\mu\text{g}/\text{ml}$  fibronectin solution. After one and three days of culture, we observed that the cells on the titanium blocks covered by nanosheets with 50 and 100  $\mu\text{m}$  groove spacings, respectively, were oriented in a direction parallel with the channels. Interestingly, the F-actin of the cells on the microgrooved nanosheet also assembled in an orientation that reflected the elongated cell shape (Figures 3b and S7). In contrast, the cells on the flat PLGA nanosheets exhibited a random arrangement. Similarly, the F-actin of these cells exhibited slightly tangled assemblies. The stress fibers in an elongated cell typically induce nuclear shape remodeling.<sup>[19]</sup> Therefore, the nuclei of the oriented cells also exhibited a preferential orientation.<sup>[20]</sup> The cell alignment was quantified by investigating the alignment of the cell nuclei (Figure 3b and S7). The cells were regarded as aligned if their nuclei were oriented within  $10^\circ$  of the direction of the grooves. Consistent with the F-actin and LIVE/DEAD staining images, the nuclei of cells on the microgrooved nanosheets indicated significant alignment. Approximately 41% and 29% of the nuclei on the nanosheets with the 50 and 100  $\mu\text{m}$  groove spacings, respectively, were aligned, whereas only 12% of the cell nuclei on the flat nanosheet were oriented in the vertical direction. Our results agree with previous reports that channels with narrow widths would be beneficial to cell alignment.<sup>[21]</sup> Intriguingly, after 7 days of culture, type I collagen (the most abundant ECM in the periosteum and bone) was detectable by immunofluorescence (Figure 3d).<sup>[2]</sup> Type I collagen secreted by cells on the microgrooved nanosheet also displayed remarkable alignment. This interesting structure is similar to ECM in natural periosteum that are highly longitudinally oriented. Previous studies confirmed that the orientation of the ECM in the periosteum has an important role in directing bone growth.<sup>[2]</sup> Therefore, our results suggest that microgrooved nanosheets could be a promising tool for developing artificial periosteum.

Encouraged by these findings, we further evaluated the osteogenic differentiation of stem cells on the titanium blocks covered by nanosheets with 50  $\mu\text{m}$  groove spacings due to their ability to regulate cell orientation. A flat PLGA nanosheet-covering titanium block and bare titanium block were used as controls. We used a conventional osteogenic medium plus 1  $\mu\text{g}/\text{ml}$  recombinant human bone morphogenetic protein (rh-BMP-2) to induce the osteogenic differentiation of ADMSCs on the nanosheets because BMP-2 is a key signal in periosteum-involved osteogenesis. After 14 days of culture, four

important osteogenic markers (Runx2/Cbfa-1, SPARC, osteocalcin, and type I collagen) were assessed by immunofluorescence (Figure 4a). Compared to the controls, the cells on the microgrooved nanosheet-covering titanium block expressed higher levels of Runx/Cbfa-1 (an early osteogenic marker that binds specific DNA sequences that activate the development of stem cells into preosteoblasts) and SPARC (also termed osteopontin, an important protein for regulating bone mineralization and bone remodeling).<sup>[21]</sup> To test the osteogenic commitment of stem cells on the microgrooved nanosheet-covering titanium block, we isolated RNA from the cells after 7 and 14 days of differentiation. Quantitative reverse transcription-polymerase chain reaction (qRT-PCR) was used to amplify the expressed transcripts from the osteogenic genes (ALP, Runx2/Cbfa-1, type I collagen, and osteocalcin) (Figure 4b). Although the cells on the bare titanium blocks expressed significantly stronger ALP (an early osteogenic marker) and osteocalcin (the most typical marker for last-stage osteogenesis and an important factor for mineralization) on Day 7, a low level of gene expression was observed in all of the groups, indicating weak osteogenic differentiation. The expression of osteogenic genes increased remarkably after 14 days of culture. The cells on the microgrooved nanosheet-covering titanium block exhibited significantly higher osteogenic commitment due to the strong expression of Runx2/Cbfa-1, type I collagen (the main template for mineralization and the most abundant protein in bone), and osteocalcin, indicating that the biomimic microgrooved nanosheets can effectively regulate the osteogenesis of cells in a manner similar to natural periosteum.<sup>[22]</sup> Recent studies have provided valuable insights into topographic cues, such as nano- and microgrooves, that effectively guide and promote the osteogenesis of osteoblasts and stem cells.<sup>[23]</sup>

The observed osteogenesis of the cells was attributed to the substrates with microgrooved motifs properly orienting the collagen filaments. Thus, our results suggest that the microgrooved PLGA nanosheet directed not only cellular alignment but also protein and gene expression levels, which is an ideal mimic of the periosteum-like microenvironment. We believe that in the clinical setting, microgrooved nanosheets will initially enhance the cellular organization and subsequently degraded after one month (Figure S8). During long period of culture of cells on microgrooved nanosheet-covering titanium blocks, microgrooved cell sheets can be generated on the titanium blocks with the degradation of PLGA nanosheets.

The stem cell laden-PLGA microgrooved nanosheets can be involved in current bone healing strategies.<sup>[3]</sup> For instance, we can cover them onto allograft bone or various artificial scaffolds or implants (e.g., titanium alloy, bioceramic porous scaffolds) that are no feasible periosteum remaining.<sup>[5]</sup> Additionally, the stem cell laden-microgrooved nanosheets also can be used as pseudo periosteum for adult autograft bone implantation, due to the decreased osteogenic potential of periosteum with age.<sup>[5]</sup>

In summary, we developed flexible “sticker-like” PLGA nanosheets with various motifs by a combination of spin coating and micropatterning. We used PLGA nanosheets with grooved micropatterns to simulate natural periosteum for bone repair therapies. The microgrooved nanosheets can be adhered onto various scaffolds and implants with a high stability and adhesiveness in aqueous conditions. This unique property

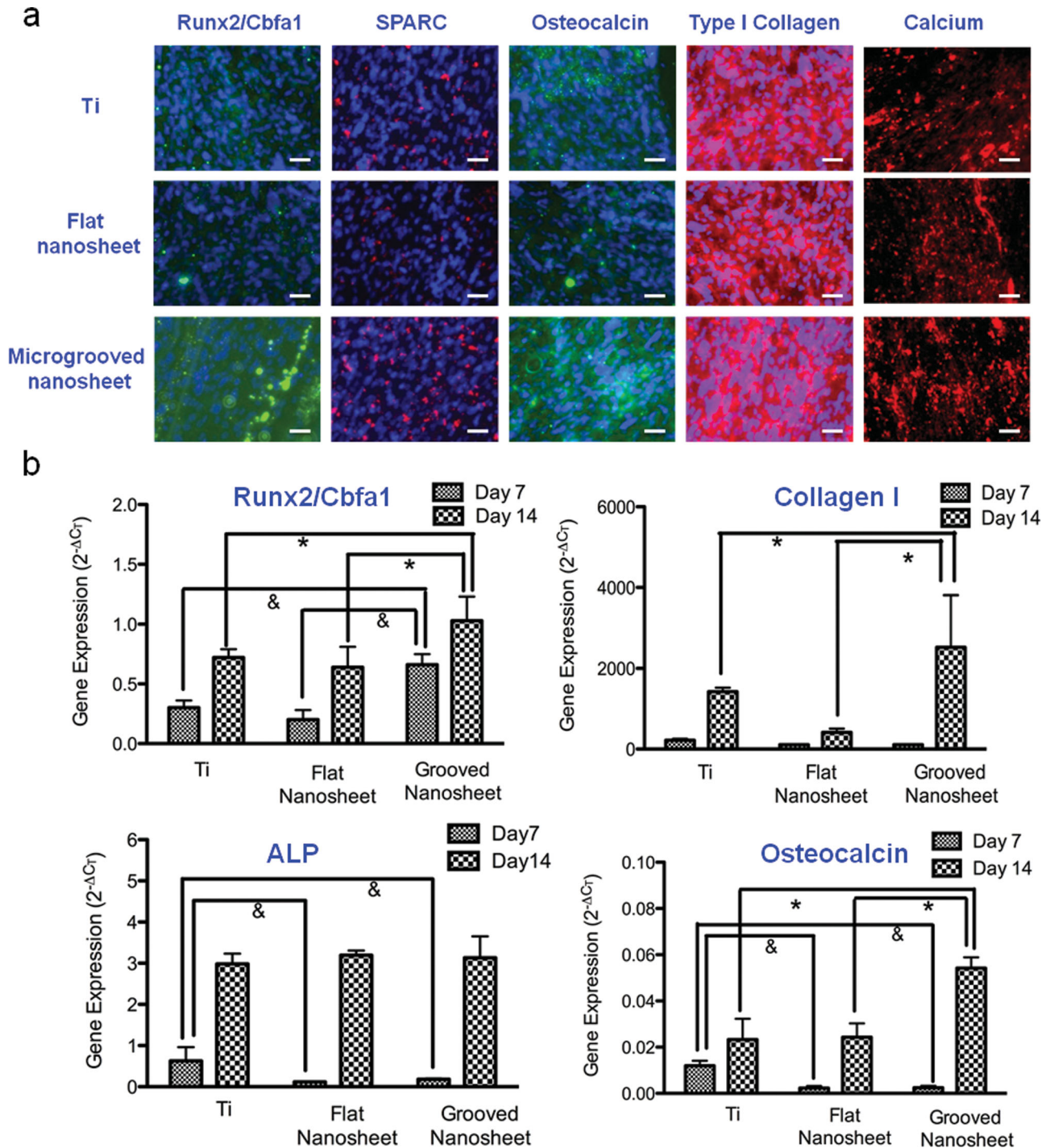


**Figure 4.** Osteogenesis of stem cells cultured on microgrooved PLGA nanosheet-covering titanium blocks, flat PLGA nanosheets-covering titanium blocks, and bare titanium blocks for 14 days. a) Immunofluorescent (nuclei were stained with DAPI) and calcium staining (scale bars: 50  $\mu\text{m}$ ) of stem cells cultured on microgrooved PLGA nanosheet-covering titanium blocks, flat PLGA nanosheets-covering titanium blocks, and bare titanium blocks for 14 days. b) Gene expression of stem cells cultured on microgrooved PLGA nanosheet-covering titanium blocks, flat PLGA nanosheets-covering titanium blocks, and bare titanium blocks for 14 days. & indicates statistical significance when compared with cells on the titanium block at 95% confidence level. \* indicates statistical significance when compared with cells on the microgrooved nanosheet-covering titanium block at 95% confidence level. The housekeeping gene  $\beta$ -actin was used as internal control for gene expression normalization.

allows the cell-laden nanosheet to remain fastened onto various bone implants during *in vitro* culturing and *in vivo* implantation. In addition, the microgrooved nanosheets can effectively

regulate the cell alignment of the stem cells cultured on them. Titanium blocks covered with microgrooved nanosheets were used to investigate the osteogenesis of stem cells. The results

suggest that the microgrooved nanosheet-covering titanium blocks effectively promote the expression of certain important osteogenic markers of the cultured stem cells. These unique features enable microgrooved “sticker-like” PLGA nanosheets to serve as stable and biomimic templates for the generation of artificial periosteal for bone repair purposes and biological studies.

## Supporting Information

Supporting Information is available from the Wiley Online Library or from the author.

## Acknowledgements

This work is supported by the World Premier International Research Center Initiative (WPI) and JSPS KAKENHI (Grant Number: 25870050 for T. F.) from MEXT, Japan. H. K. W. acknowledges the support of the Hong Kong RGC (GRF 604509 and GRF 605210).

Received: November 25, 2013

Revised: January 5, 2014

Published online: March 11, 2014

- [1] a) J. M. Karp, L. S. Ferreira, A. Khademhosseini, A. H. Kwon, J. Yeh, R. Langer, *Stem Cells* **2006**, *24*, 835; b) J. P. Vacanti, R. Langer, *Lancet* **1999**, *354*, S132; c) V. Prasad Shastri, *Adv. Mater.* **2009**, *21*, 3246; d) A. Khademhosseini, J. Vacanti, R. Langer, *Sci. Am.* **2009**, *21*, 3307; e) L. M. Boyden, J. Mao, J. Belsky, L. Mitzner, A. Farhi, M. A. Mitnick, D. Wu, K. Insogna, R. P. Lifton, *N. Engl. J. Med.* **2002**, *346*, 1513.
- [2] a) E. Bell, B. Ivarsson, C. Merrill, *Proc. Natl. Acad. Sci. U. S. A.* **1979**, *76*, 1274; b) G. Augustin, A. Antabak, S. Davila, *Injury* **2007**, *38*, 1115; c) E. A. Tonna, *Nature* **1958**, *181*, 486; d) M. Caballero, C. R. Reed, G. Madan, J. R. van Aalst, *Ann. Plast. Surg.* **2010**, *64*, 605.
- [3] a) P. Petrochenko, R. J. Narayan, J. Long, *Term. Eff. Med. Implants* **2010**, *20*, 303; b) L. Uddstromer, *Scand. J. Plast. Reconstr. Surg.* **1978**, *12*, 195; c) J. Foolen, C. van Donkelaar, N. Nowlan, P. Murphy, R. Huiskes, K. Ito, *J. Orthop. Res.* **2008**, *26*, 1263; d) E. A. Tonna, N. Pillsbury, *Nature* **1959**, *183*, 337; e) W. Fan, R. Crawford, Y. Xiao, *Bone* **2008**, *42*, 81.
- [4] a) E. Seeman, *N. Engl. J. Med.* **2003**, *349*, 320; b) C. Colnot, X. Zhang, M. L. Knothe Tate, *J. Orthop Res.* **2012**, *30*, 1869.
- [5] a) B. Schönmeier, N. Clavin, T. Abraham, V. Longo, B. J. Mehrara, *Tissue Eng Part A* **2009**, *15*, 1833; b) Y. Zhou, F. Chen, S. T. Ho, M. A. Woodruff, T. M. Lim, D. W. Huttmacher, *Biomaterials* **2007**, *28*, 814; c) M. D. Hoffman, C. Xie, X. Zhang, D. S. W. Benoit, *Biomaterials* **2013**, *34*, 8887.
- [6] a) T. Fujie, Y. Okamura, S. Takeoka, *Adv. Mater.* **2007**, *19*, 3549; b) H. Watanabe, A. Fujimoto, A. Takahara, *Soft Matter*, **2011**, *7*, 1856; c) T. Fujie, Y. Kawamoto, H. Haniuda, A. Saito, K. Kabata, Y. Honda, E. Ohmori, T. Asahi, S. Takeoka, *Macromolecules* **2012**, *46*, 395.
- [7] a) C. Jiang, V. V. Tsukruk, *Adv. Mater.* **2006**, *18*, 829; b) T. Fujie, N. Matsutani, M. Kinoshita, Y. Okamura, A. Saito, S. Takeoka, *Adv. Funct. Mater.* **2009**, *19*, 2560; c) X. Peng, J. Jin, Y. Nakamura, T. Ohno, I. Ichinose, *I. Nature Nanotech.* **2009**, *4*, 353.
- [8] a) H. Miyazaki, M. Kinoshita, A. Saito, T. Fujie, K. Kabata, E. Hara, S. Ono, S. Takeoka, D. Saitoh, *Wound Repair Regen.*, **2012**, *20*, 573; b) Y. Okamura, K. Kataba, M. Kinoshita, H. Miyazaki, A. Saito, T. Fujie, S. Ohtsubo, D. Saitoh, S. Takeoka, *Adv. Mater.* **2013**, *25*, 545.
- [9] a) X. Shi, S. Chen, J. Zhou, H. Yu, L. Li, H. Wu, *Adv. Funct. Mater.* **2012**, *22*, 3799; b) X. Shi, Y. Wang, R. R. Varshney, L. Ren, F. Zhang, D. A. Wang, *Biomaterials*, **2009**, *30*, 3996.
- [10] a) H. Tekin, J. G. Sanchez, C. Landeros, K. Dubbin, R. Langer, A. Khademhosseini, *Adv. Mater.* **2012**, *24*, 5543; b) P. Zorlutuna, N. Annabi, G. Camci-Unal, M. Nikkhah, J. M. Cha, J. W. Nichol, A. Manbachi, H. Bae, S. Chen, A. Khademhosseini, *Adv. Mater.* **2012**, *24*, 1782.
- [11] a) N. Annabi, K. Tsang, S. M. Mithieux, M. Nikkhah, A. Ameri, A. Khademhosseini, A. S. Weiss, *Adv. Funct. Mater.* **2013**, *23*, 4950; b) O. Jeon, E. Alsberg, *Adv. Funct. Mater.* **2013**, *23*, 4765; c) P. Gong, W. Zheng, Z. Huang, W. Zhang, D. Xiao, X. Jiang, *Adv. Funct. Mater.* **2013**, *23*, 42.
- [12] R. Gauvin, A. Khademhosseini, *ACS Nano* **2011**, *5*, 4258.
- [13] a) M. Théry, *J. Cell Sci.* **2010**, *123*, 4201; b) P. Zorlutuna, A. Tezcaner, V. Hasirci, *J. Biomater. Sci. Polym. Ed.* **2008**, *19*, 399.
- [14] a) T. Fujie, S. Furutate, D. Niwa, S. Takeoka, *Soft Matter* **2010**, *6*, 4672; b) T. Fujie, S. Ahadian, H. Liu, H. Chang, S. Ostrovidov, H. Wu, H. Bae, K. Nakajima, H. Kaji, A. Khademhosseini, *Nano Lett.* **2013**, *13*, 3185.
- [15] R. Langer, J. P. Vacanti, C. A. Vacanti, A. Atala, L. E. Freed, G. Vunjak-Novakovic, *Tissue Eng.* **1995**, *1*, 151.
- [16] a) K. Matsuzaka, X. F. Walboomers, J. E. Ruijter, J. A. Jansen, *Biomaterials* **1999**, *20*, 1293; b) X. Shi, S. Chen, Y. Zhao, C. Lai, H. Wu, *Adv. Healthcare Mater.* **2013**, *2*, 1229; c) X. Lu, Y. Leng, *J. Biomed. Mater. Res. B. Appl. Biomater.* **2009**, *90*, 438.
- [17] a) C. Liang, H. Wang, J. Yang, Y. Cai, X. Hu, Y. Yang, B. Li, H. Li, H. Li, C. Li, X. Yang, *ACS Appl. Mater. Interfaces* **2013**, *5*, 8179; b) H. W. Chien, W. B. Tsai, *Acta Biomater.* **2012**, *8*, 3678.
- [18] S. Law, S. Chaudhuri, *Am. J. Stem Cells* **2013**, *2*, 22.
- [19] M. Versaavel, T. Grevesse, S. Gabriele, *Nat. Commun.* **2012**, *3*, 671.
- [20] a) M. Nikkhah, N. Eshak, P. Zorlutuna, N. Annabi, M. Castello, K. Kim, A. Dolatshahi-Pirouz, F. Edalat, H. Bae, Y. Yang, A. Khademhosseini, *Biomaterials* **2012**, *33*, 9009; b) X. Shi, S. Chen, Y. Zhao, C. Lai, H. Wu, *Adv. Healthcare Mater.* **2013**, *2*, 1229.
- [21] a) A. K. Gaharwar, S. M. Mihaila, A. Swami, A. Patel, S. Sant, R. L. Reis, A. P. Marques, M. E. Gomes, A. Khademhosseini, *Adv. Mater.* **2013**, *24*, 3329.
- [22] H. M. Kronenberg, *Nature* **2003**, *423*, 332.
- [23] a) L. Prodanov, J. te Riet, E. Lamers, M. Domanski, R. Luttge, J. J. W. A. van Loon, J. A. Jansen, X. F. Walboomers, *Biomaterials* **2010**, *31*, 7758; b) S. D. Subramony, B. R. Dargis, M. Castillo, E. U. Azeloglu, M. S. Tracey, A. Su, H. H. Lu, *Biomaterials* **2013**, *34*, 1942.